Approach to achieving a p-type transparent conducting oxide: Doping of bismuth-alloyed Ga₂O₃ with a strongly correlated band edge state

Xuefen Cai, 1,2 Fernando P. Sabino, Anderson Janotti, and Su-Huai Wei, 1,7 ¹Beijing Computational Science Research Center, Beijing 100094, China ²Department of Materials Science and Engineering, University of Delaware, Newark, Delaware 19716, USA

(Received 26 October 2020; revised 10 January 2021; accepted 10 March 2021; published 22 March 2021)

P-type doping in oxides is usually difficult due to their low valence-band energy. In order to make them p type, the electronic structure of the oxides should be fundamentally changed; that is, the occupied valence band should be raised significantly. Here, using first-principles calculations, we propose that by adding a small amount of Bi₂O₃ into Ga₂O₃ to form dilute (Bi_xGa_{1-x})₂O₃ alloys and, more importantly, with properly chosen dopants, we can achieve efficient p-type doping in a transparent oxide. We show that adding a few percent of Bi to Ga_2O_3 leads to an intermediate valence band that is sufficiently high in energy to facilitate p-type doping; however, the commonly expected shallow acceptors, Mg and Zn substitution on the Ga site (MgGa and ZnGa), are still deep acceptors, whereas the expected deep acceptor, CuGa, actually creates a relatively shallow level in $(Bi_xGa_{1-x})_2O_3$ alloys. This trend is opposite to what is found in pure Ga_2O_3 . The puzzling behavior of the acceptor levels in the $(Bi_xGa_{1-x})_2O_3$ alloys is attributed to the polaronic character of the holes in the Zn- and Mg-doped cases, and the decoupling of the hole state and the valence-band edge in the Cu-doped case. This understanding provides insights into the realization of p-type doping in dilute $(B_i Ga_{1-x})_2 O_3$ alloys and paves a way to dope semiconductor materials with a strongly correlated band edge state, i.e., materials with a tendency to form polaronic acceptor or donor states.

DOI: 10.1103/PhysRevB.103.115205

I. INTRODUCTION

p-type doping in wide band gap semiconductors is attractive due to its many interesting technological applications, but p-type doping in oxides is difficult due to their low valence-band energy [1]. This is the case of Ga₂O₃, which has attracted great attention in the last few years due to its potential application in high-power electronics, ultrasensitive gas detectors, and various optoelectronic devices [2–5]. Ga_2O_3 crystallizes in five different polymorphs denoted by α , β , γ , δ , and ε , among which the base-centered monoclinic β -Ga₂O₃ with symmetry group C2/m is the most stable form at ambient conditions [6,7]. The conventional unit cell of β -Ga₂O₃ contains four formula units (20 atoms), with two crystallographic nonequivalent Ga sites, one with tetrahedral (Ga-I) and the other with octahedral (Ga-II) coordination geometry, and three nonequivalent O sites located at 4i(x, 0, z), one with fourfold coordination (O-I), and two with threefol coordination (O-II and O-III).

 Ga_2O_3 in the β phase has an indirect band gap of \sim 4.7 eV, compared with the direct band gap that is only 30-40 meV higher in energy [4,8]. It is relatively easy to dope Ga_2O_3 n type by substituting group-IV elements (Si, Ge, and Sn) on the Ga sites, with controllable carrier concentrations in the range of 10^{16} – 10^{19} cm⁻³ [3,9–11]. However, it has been shown that it is very difficult or even impossible to dope Ga₂O₃ p type, like many other wide band gap oxide semiconductors [12]. For the potential shallow acceptor candidate dopants, such as Zn, Mg, and N, the reported transition energy levels are higher than 1 eV above the valence band [12–14]. In short, Ga₂O₃ is a promising transparent conducting oxide (TCO) material with high levels of *n*-type doping, but *p*-type doping has not yet been realized.

So far, all the trademark TCOs are n type, such as Sndoped In₂O₃ (ITO), F-doped SnO₂ (FTO), and Al-doped ZnO (AZO). The lack of p-type TCOs has limited the design flexibility of optoelectronic devices such as solar cells, LEDs, and transparent field-effect transistors [15-17]. A possible avenue for overcoming this limitation is to raise the valence band of the material [1,18]. Driven by this concept, a variety of candidates for p-type TCOs have emerged, such as the Cu-based materials $(3d^{10})$, transition metal containing oxides $(3d^n)$, post transition metal oxides (ns^2) , and layered oxychalcogenides (LaCuOCh, Ch = S and Se) [15–17,19–21]. Enlightened by these findings and guided by the doping limit rules [1], we show in this work that by adding a small amount of Bi₂O₃ into Ga₂O₃ to form dilute (Bi_xGa_{1-x})₂O₃ alloys and, more importantly, properly choosing doping impurities, we can achieve efficient p-type doping in these transparent oxides.

Results of first-principles calculations show that the valence-band maximum (VBM) of the dilute (Bi_rGa_{1-r})₂O₃ alloy is significantly pushed up by more than 1.6 eV compared with the host material Ga₂O₃, making it easier to achieve p-type doping in the $(Bi_xGa_{1-x})_2O_3$ alloy according to the doping limit rules [1]. It is expected that if the localized defect

^{*}ianotti@udel.edu

[†]suhuaiwei@csrc.ac.cn

TABLE I. Calculated and experimental lattice parameters $(a, b, c, \text{ and } \beta)$ and band gap (E_g) of β -Ga₂O₃ and α -Bi₂O₃.

| | | a (Å) | b (Å) | c (Å) | β | $E_g(eV)$ |
|--|---------------|-------|-------|-------|---------|-----------|
| β -Ga ₂ O ₃ | Calc. | 12.29 | 3.05 | 5.81 | 103.72° | 4.84 |
| | Expt. [6,8] | 12.21 | 3.04 | 5.80 | 103.83° | 4.90 |
| α -Bi ₂ O ₃ | Calc. | 5.86 | 8.11 | 7.44 | 112.50° | 3.56 |
| | Expt. [24,25] | 5.83 | 8.14 | 7.48 | 112.93° | 3.71 |

level is uncorrelated with the VBM, when the VBM shifts up by the addition of Bi into Ga₂O₃, the acceptor transition level can change from deep in the host material to shallow in the alloy. To test this concept, we considered Mg, Zn, and Cu substitutions on the Ga site (Mg_{Ga}, Zn_{Ga}, and Cu_{Ga}) in dilute $(Bi_xGa_{1-x})_2O_3$. Interestingly, we find that Mg_{Ga} and Zn_{Ga} are also deep acceptors in the alloy, even though they are chemically similar to Ga. On the other hand, we find that CuGa induces a shallow acceptor level, making it a good candidate for producing p-type $(Bi_xGa_{1-x})_2O_3$. This trend is opposite to the results found in Ga₂O₃. These unexpected results are explained by the strong correlation of the VBM state which has localized Bi 6s and O 2p orbital characters and the consequent polaronic effects. The concepts developed here are important for understanding doping in other related semiconductors with a strongly correlated band edge state.

II. COMPUTATIONAL METHOD

Our first-principles calculations are based on the projector augmented wave (PAW) method and density functional theory (DFT) with the HSE06 hybrid functional [22] as implemented in the VASP code [23]. We use a cutoff energy of 520 eV for the plane-wave basis set and PAW potentials. For structural optimization, atomic positions are fully relaxed until the Hellmann-Feynman force on each atom is less than 0.01 eV/Å. For the HSE06 calculations, we set the Hartree-Fock exchange mixing parameter α to 34%. As shown in Table I, the calculated structural parameters and band gaps of β -Ga₂O₃ and α -Bi₂O₃ are in good agreement with the experimental data [6,8,24,26]. Note that for monoclinic α -Bi₂O₃, space group $P2_1/c$ [24], which is the most stable phase at room temperature, there are two types of cation environments with different coordination to anion atoms: Bi-I, which is fivefold coordinated, and Bi-II, which is sixfold coordinated.

To simulate random β -(Bi_xGa_{1-x})₂O₃ alloys, we construct quasirandom structures (SQS) [27] based on a supercell of 160 atoms, where one, two, four, and eight Ga atoms are replaced by Bi (x = 1/64, 1/32, 1/16, and 1/8, respectively). We only consider the β phase alloy here because it has lower energy at these low Bi concentrations. Having the two different bonding environments of Ga in β -Ga₂O₃ poses the question of which cation site Bi prefers to occupy. We have tested the two configurations and found that the Bi atom favors the sixfold coordinated sites, with a total energy difference of 635 meV per Bi between the two configurations. Thus, we consider dilute (Bi_xGa_{1-x})₂O₃ alloys where Bi only occupies the octahedral Ga-II sites. For exploring p-type doping, we consider here only the 160-atom (Bi_xGa_{1-x})₂O₃ alloy with x = 1/8 and x = 0 (Ga₂O₃) with the dopants substituting on the Ga

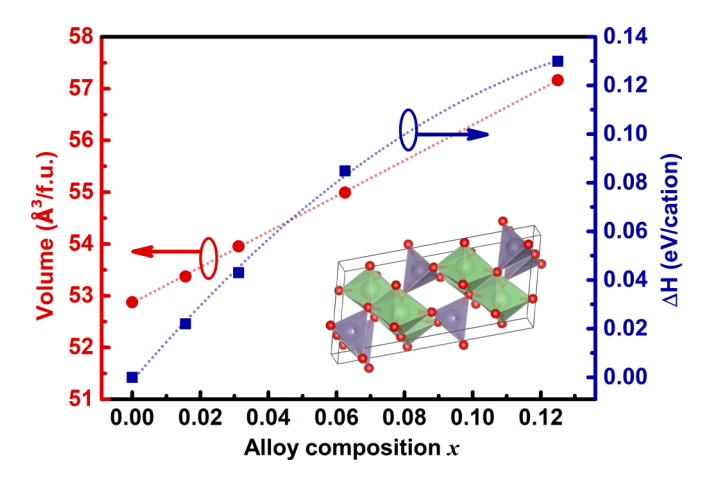


FIG. 1. Volume per formula unit (red circles) and mixing enthalpy per cation ΔH (blue squares) of dilute (Bi_xGa_{1-x})₂O₃ alloys as a function of Bi content x in the monoclinic β structure of the Ga₂O₃ parent compound. The straight red line indicates good agreement with Vegard's law and the blue curve is for guiding the eye. The inset shows the monoclinic β -Ga₂O₃ unit cell.

site $(Mg_{Ga}, Zn_{Ga}, and Cu_{Ga})$. Spin-polarized calculations are carried out for systems with unpaired electrons. The defect formation energy and transition energy levels are calculated as described in the literature [28,29]. Validation of the defect level position was attested by performing convergence calculations with larger supercell and different mixing parameters in the HSE calculations [30,31], the results of which are included in the Supplemental Material [32].

III. RESULTS AND DISCUSSION

When adding Bi to β -Ga₂O₃ to form a β -(Bi_xGa_{1-x})₂O₃ alloy, the alloy volume per formula unit expands as shown in Fig. 1, which can be attributed to the larger atomic size of Bi compared to Ga. Our results indicate that the volume of the alloy in the monoclinic β structure closely follows Vegard's law [27] in the dilute concentration range. To examine the stability of these alloys, we computed the mixing enthalpy (ΔH) of β -(Bi_xGa_{1-x})₂O₃ for different Bi concentrations, defined by

$$\Delta H(x) = E_{(\text{Bi}_x\text{Ga}_{1-x}),\text{O}_3} - (1-x)E_{\text{Ga}_2\text{O}_3} - xE_{\text{Bi}_2\text{O}_3}, \quad (1)$$

where $E_{\text{Ga}_2\text{O}_3}$ and $E_{\text{Bi}_2\text{O}_3}$ are the total energies of β -Ga₂O₃ and α -Bi₂O₃, respectively, and $E_{(\text{Bi}_x\text{Ga}_{1-x})_2\text{O}_3}$ is the total energy of the $(\text{Bi}_x\text{Ga}_{1-x})_2\text{O}_3$ alloy. The results are marked as blue squares in Fig. 1. Similar calculations have also been done for α -(Bi_xGa_{1-x})₂O₃, which confirmed our expectation that $(\text{Bi}_x\text{Ga}_{1-x})_2\text{O}_3$ alloys energetically prefer the monoclinic β phase for all Bi concentrations in the considered dilute regime.

Figure 2(a) shows a schematic of the electronic band structure of dilute $(Bi_xGa_{1-x})_2O_3$ alloys with Bi concentration x = 0, 1/64, 1/32, 1/16, and 1/8. Note that for these dilute Bi alloys, the O 2p bands change only slightly with x, so we use these O 2p bands as reference for easy inspection. It is observed that (i) an occupied intermediate valence band (shown in orange) emerges after the incorporation of Bi; (ii) the bandwidth of the intermediate valence band becomes larger with the increase of Bi concentration; (iii) the band gap of the alloy increases with the Bi concentration x, and the

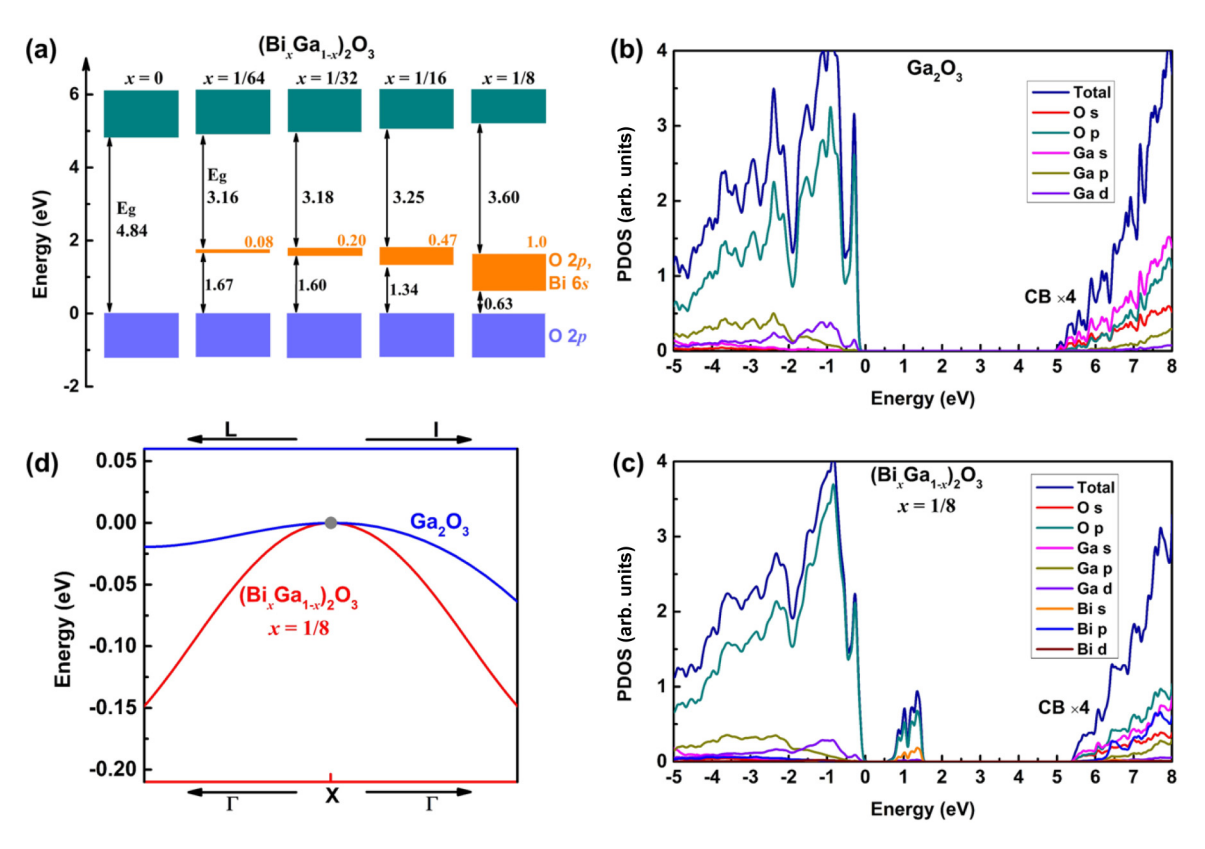


FIG. 2. (a) Schematic representation of the electronic band structure of β -(Bi_xGa_{1-x})₂O₃ alloys with x = 1/64, 1/32, 1/16, and 1/8, compared to that of β -Ga₂O₃. The calculated total and partial density of states for (b) Ga₂O₃ and (c) the (Bi_xGa_{1-x})₂O₃ alloy with x = 1/8. The zero in the energy axis is placed at the VBM of Ga₂O₃. The PDOS intensity in the conduction band (CB) range is artificially enlarged by 4 times for better visualization. (d) The first valence-band edge close to its maximum along the *L-I* line for Ga₂O₃ (blue line) and the Γ -*X*- Γ line for the (Bi_xGa_{1-x})₂O₃ alloy with x = 1/8 (red line). The gray circle indicates the VBM of both structures.

upshift of the conduction band minimum (CBM) is attributed to the level repulsion between the CBM and the intermediate valence band. The detailed projected density of states (PDOS) for Ga_2O_3 and the $(Bi_xGa_{1-x})_2O_3$ alloy with x = 1/8 are given in Figs. 2(b) and 2(c). The valence band maximum (VBM) state of Ga_2O_3 is dominated by the O 2p orbital, while the CBM is mainly composed of Ga 4s and O 2s states. For the $(Bi_xGa_{1-x})_2O_3$ alloy with x = 1/8, an occupied intermediate valence band derived from hybridization of O 2p and Bi 6s orbitals emerges; that is, the top of the valence band is significantly raised, by more than 1.6 eV. The bandwidth of the intermediate valence band for the alloy with x = 1/8 is approximately 1.0 eV. For comparison, we also specifically depicted the first valence-band edge in the vicinity of its maximum for Ga_2O_3 and the alloy with x = 1/8 in Fig. 2(d), where the former one is along the *L-I* path, while the latter one is along the Γ -X- Γ path. The VBM of Ga₂O₃ locates on the L-I path [33]. We set the VBM energy as zero in both cases for easy comparison. The corresponding calculated hole effective mass of the VBM for Ga_2O_3 is $3.13m_0$, which lies within the reported range [34,35]. As for the alloy with x = 1/8, the calculated hole effective mass at the VBM is $0.74m_0$, indicating that a higher electrical conductivity in the $(Bi_xGa_{1-x})_2O_3$ alloy could be obtained than in Ga₂O₃. It is noted that the band gaps of these dilute (Bi_xGa_{1-x})₂O₃ alloys remain wider than 3.1 eV, which ensures high optical transparency in the visible and near-infrared regions of the spectrum. Therefore,

finding shallow acceptor impurities in β -(Bi_xGa_{1-x})₂O₃ alloys will potentially lead to the so desired *p*-type TCO.

We first examined on which lattice sites the acceptor impurities will prefer to incorporate, since there are many different local environments in the $(Bi_xGa_{1-x})_2O_3$ alloy. We tested substituting a neutral Zn impurity on all possible Ga sites in the $(Bi_xGa_{1-x})_2O_3$ alloy, comparing the total energy as a function of distance to the Bi atom. The results are shown in Fig. S1 of the Supplemental Material [32]. We find that, in general, the total energy increases as the distance between $Zn_{Ga}{}^0$ and Bi atoms increases; i.e., the Zn acceptor energetically prefers to stay close to the Bi atom. Similar behavior is obtained for the Mg and Cu acceptor impurities.

To illustrate the properties of the dopants in the $(Bi_xGa_{1-x})_2O_3$, we chose $(Bi_xGa_{1-x})_2O_3$ alloys with x = 1/8, and x = 0 (Ga_2O_3) for comparison. For the alloy with x = 1/8, which is described by the special quasirandom structure model, we observe that the width of the intermediate valence band is fairly large, and the charge distribution associated with the intermediate valence band is quite uniform. As discussed above, we only considered one of the substitutional sites next to one of the Bi in the alloy.

Figure 3 depicts the formation energy for Mg, Zn, and Cu acceptors as a function of the Fermi level position under O-rich conditions, in which the defect formation energies are lower than that under O-poor conditions. The range of Fermi level is from VBM to CBM, that is, from 0 to 4.84 eV for

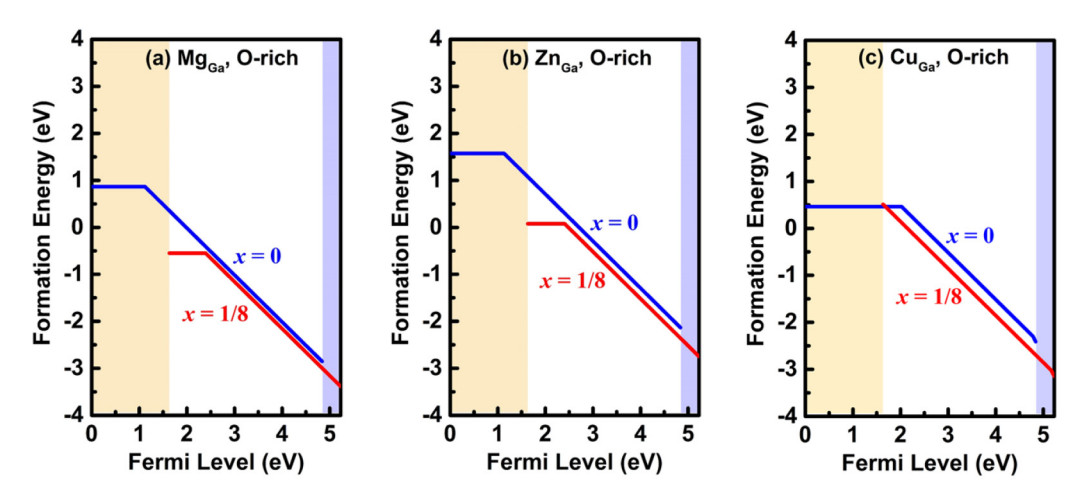


FIG. 3. Calculated formation energies for Mg_{Ga} , Zn_{Ga} , and Cu_{Ga} in $(Bi_xGa_{1-x})_2O_3$ alloys with x=0 (Ga_2O_3) and x=1/8 under O-rich conditions as a function of Fermi level. Note the different ranges of the Fermi level in the two systems. The zero of the Fermi level is at the VBM of pure Ga_2O_3 . The dopant chemical potentials are limited by the formation of MgO, ZnO, and CuO, respectively.

 Ga_2O_3 and from 1.63 to 5.23 eV for the $(Bi_xGa_{1-x})_2O_3$ alloy with x = 1/8. The shaded regions correspond to Fermi level positions below the VBM (yellow) of the $(Bi_xGa_{1-x})_2O_3$ alloy and above the CBM (purple) of Ga_2O_3 .

We first discuss the properties of Mg_{Ga} and Zn_{Ga} dopants. The formation energies of Mg_{Ga} are lower than that of Zn_{Ga} in both Ga_2O_3 and $(Bi_xGa_{1-x})_2O_3$. This can be attributed to the closer ionic radius between Mg and Ga than between Zn and Ga [36], and also the larger bonding strength between Mg and O than that between Zn and O, reflected in the differences in the formation enthalpy of MgO and ZnO. In Ga₂O₃, the (0/–1) transition energy levels of Mg_{Ga} and Zn_{Ga} occur at 1.1 eV above the VBM, in agreement with previous studies [12–14], and can attributed to the low-lying VBM of Ga₂O₃. Unfortunately, Mg_{Ga} and Zn_{Ga} also lead to deep acceptor transition levels in $(Bi_xGa_{1-x})_2O_3$, at ~ 0.8 eV above the intermediate valence band in the alloy with x = 1/8. Compared to Ga_2O_3 , it is easy to see from the results in Fig. 3 that the acceptor levels of Mg_{Ga} and Zn_{Ga} are closer to the valence band in the $(Bi_xGa_{1-x})_2O_3$ alloy than in Ga_2O_3 .

The deep transition levels of MgGa and ZnGa in the alloy with x = 1/8 apparently contradict the expectation that these impurities would act as shallow acceptors and lead to efficient p-type doping in the $(Bi_xGa_{1-x})_2O_3$ alloy since the VBM now is pushed up by more than 1.6 eV (cf. Fig. 2), assuming that the hole state would be fixed in an absolute energy scale. To understand this unexpected result, it is informative to inspect the charge density distribution of the single-particle hole state of the neutral acceptor impurity in both Ga_2O_3 and $(Bi_xGa_{1-x})_2O_3$ alloy. The case of Zn_{Ga} is shown in Figs. 4(a) and 4(b). In Ga₂O₃, the impurity-induced hole state is localized mostly on a single oxygen site adjacent to the substitutional Zn atom, indicating a hole polaronic behavior [13,37], which is part of the reason that Zn is not an efficient p-type dopant in Ga_2O_3 . In the case of $(Bi_xGa_{1-x})_2O_3$ alloy, the single-particle hole state related to Zn_{Ga}^{0} is localized around the Bi atom next to the impurity rather than on an O atom next to Zn as in Ga₂O₃. The same behavior is also observed for Mg_{Ga}. That is to say, the wave function of the Zn_{Ga} impurity state is coupled to its respective VBM state in both Ga_2O_3 and $(Bi_xGa_{1-x})_2O_3$, with characteristics of a polaronic state. As the VBM shifts up in energy, the polaronic state energy also shifts upwards, which explains why Mg or Zn doping will not lead to efficient *p*-type conductivity in $(Bi_xGa_{1-x})_2O_3$ alloys.

The reason that the hole is bounded to the Bi site in Zn- and Mg-doped (Bi_xGa_{1-x})₂O₃ is because the Zn and Mg impurity level in Ga_2O_3 is lower than the Bi level. In this case, the hole will float to the VBM and lead to a polaronic defect level. As the VBM shifts up due to alloying with Bi, the energy of the polaronic state also shifts up in energy, and leads to a deep transition energy level inside the band gap. To avoid this undesirable effect related to the strong correlation of the valence band, we now turn to Cu_{Ga} in Ga_2O_3 and $(Bi_xGa_{1-x})_2O_3$. Cu substituting on a Ga site is expected to be a double acceptor in Ga_2O_3 with deep level due to its active d-orbital energy. Our calculations show that the (0/-1) transition energy level of Cu_{Ga} occurs at 2.02 eV above the VBM in Ga_2O_3 , as seen

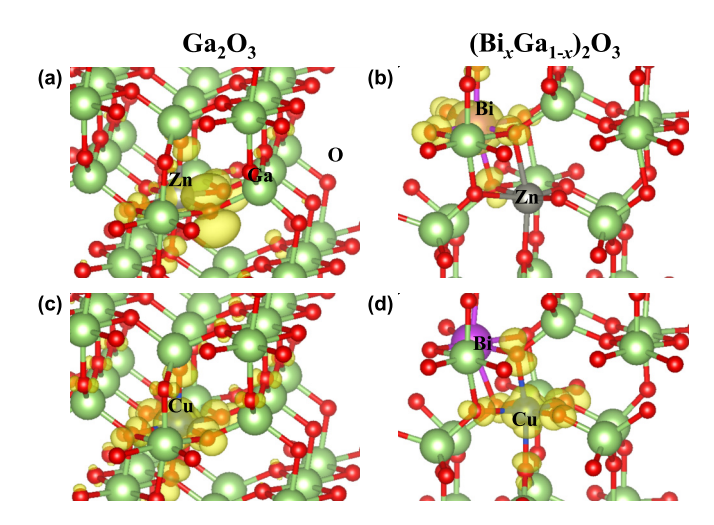


FIG. 4. Charge density distribution (yellow: isosurface of $0.005\,e/\mathrm{bohr^3}$) for hole state related to charge neutral (a) $\mathrm{Zn_{Ga}}^0$, (c) $\mathrm{Cu_{Ga}}^0$ in pure $\mathrm{Ga_2O_3}$, as well as (b) $\mathrm{Zn_{Ga}}^0$ and (d) $\mathrm{Cu_{Ga}}^0$ in $(\mathrm{Bi}_x\mathrm{Ga}_{1-x})_2\mathrm{O_3}$ with x=1/8.

in Fig. 3(c), and the (-/2-) level occurs at much higher energy, at 64 meV below the CBM. Previous works on Cu-doped Ga_2O_3 [38,39] have shown an emission peak at \sim 2.5 eV, indicating that Cu induces a deep level. We also note that the (0/-1) transition energy level of Cu_{Ga} in Ga_2O_3 occurs at higher energy than the top of the Bi-derived valence band in dilute $(Bi_xGa_{1-x})_2O_3$ alloys. Because of this, unlike Zn_{Ga} and Mg_{Ga} , the Cu_{Ga} -derived defect state is not coupled to the Bi-derived VBM, with the holes localized mainly on the Cu impurity site instead of on the Bi or O atoms as shown in Figs. 4(c) and 4(d). Due to this decoupling, we find that Cu_{Ga} leads to a shallow (0/-1) transition level in the $(Bi_xGa_{1-x})_2O_3$ alloy [cf. Fig. 3(c)].

This interesting behavior of the Cu impurity in Ga₂O₃ and dilute (Bi_xGa_{1-x})₂O₃ alloys gives us insight on how to dope materials with a strongly correlated band edge state p or ntype. In these systems, the valence and/or conduction-band edges are correlated and can form polaronic states. Using the case of p-type doping as example, by introducing a substitutional impurity such as Cu, if the Cu-related states are higher than and decoupled from the VBM of the host material, there will be large flexibility to tune the energy levels of the host VBM and defect state independently to make the acceptor level sufficiently close to the VBM of the host material. An analogous situation can be envisaged for identifying an impurity for *n*-type doping of materials with strongly correlated conduction bands. In this case, the donor state must be decoupled from the CBM of the host material, which happens when the donor level is located slightly below that of the CBM, so it could pin the donor transition level near or close to the CBM.

IV. CONCLUSION

In summary, we studied the electronic structure and doping properties of acceptor-doped dilute $(Bi_xGa_{1-x})_2O_3$ alloys

using first-principles hybrid functional calculations aiming at developing p-type TCOs. The VBM in the $(Bi_xGa_{1-x})_2O_3$ alloy is significantly higher than that in the parent compound Ga₂O₃, facilitating *p*-type doping. Contrary to common expectation, we show that Mg_{Ga} and Zn_{Ga} still lead to deep acceptor levels in the alloy, as in Ga₂O₃, whereas Cu_{Ga} leads to a shallow (0/-1) acceptor level, making it a good candidate for enabling p-type conductivity in the $(Bi_rGa_{1-r})_2O_3$ alloys. This unusual trend is explained by the hole state associated with Zn and Mg being coupled with the Bi-derived VBM state, whereas the Cu impurity state is decoupled from the VBM of the host material, giving us insight on how to dope systems with a strongly correlated band edge state. Considering the wide band gap $E_g > 3.1 \,\text{eV}$ of the dilute (Bi_xGa_{1-x})₂O₃ alloys, our work indicates that Cu doping of dilute $(Bi_xGa_{1-x})_2O_3$ alloys is a promising route to obtaining a p-type TCO, paving the way for a range of alternative applications.

ACKNOWLEDGMENTS

This work was supported by the Nature Science Foundation of China (Grants No. 11634003, No. 11991060, and No. U1930402), the Key Research & Development Program of Beijing (Grant No. Z181100005118003), the National Science Foundation under the Early Career Development Program No. DMR-1652994, and the China Scholarship Council (Grant No. 201904890014). We also express thanks for the computational support from the Beijing Computational Science Research Center (CSRC), and the XSEDE supercomputer facility under National Science Foundation Grant No. ACI-1053575.

- [11] N. Moser, J. McCandless, A. Crespo, K. Leedy, A. Green, A. Neal, S. Mou, E. Ahmadi, J. Speck, and K. Chabak, Gedoped β-Ga₂O₃ MOSFETs, IEEE Electron. Device Lett. 38, 775 (2017).
- [12] A. Kyrtsos, M. Matsubara, and E. Bellotti, On the feasibility of p-type Ga₂O₃, Appl. Phys. Lett. 112, 032108 (2018).

^[1] S.-H. Wei, Overcoming the doping bottleneck in semiconductors, Comput. Mater. Sci. **30**, 337 (2004).

^[2] M. Baldini, Z. Galazka, and G. Wagner, Recent progress in the growth of β -Ga₂O₃ for power electronics applications, Mater. Sci. Semicond. Process. **78**, 132 (2018).

^[3] M. Higashiwaki, H. Murakami, Y. Kumagai, and A. Kuramata, Current status of Ga₂O₃ power devices, Jpn. J. Appl. Phys. 55, 1202A1 (2016).

^[4] S. J. Pearton, J. Yang, P. H. Cary, F. Ren, J. Kim, M. J. Tadjer, and M. A. Mastro, A review of Ga₂O₃ materials, processing, and devices, Appl. Phys. Rev. 5, 011301 (2018).

^[5] J. Y. Tsao, S. Chowdhury, M. A. Hollis, D. Jena, N. M. Johnson, K. A. Jones, R. J. Kaplar, S. Rajan, C. G. Van de Walle, E. Bellotti, C. L. Chua, R. Collazo, M. E. Coltrin, J. A. Cooper, K. R. Evans, S. Graham, T. A. Grotjohn, E. R. Heller, M. Higashiwaki, M. S. Islam *et al.*, Ultrawide-bandgap semiconductors: Research opportunities and challenges, Adv. Electron. Mater. 4, 1600501 (2018).

^[6] J. Åhman, G. Svensson, and J. Albertsson, A reinvestigation of β-gallium oxide, Acta Crystallogr., Sect. C 52, 1336 (1996).

^[7] H. He, M. A. Blanco, and R. Pandey, Electronic and thermodynamic properties of β-Ga₂O₃, Appl. Phys. Lett. 88, 261904 (2006).

^[8] M. Orita, H. Ohta, M. Hirano, and H. Hosono, Deep-ultraviolet transparent conductive β -Ga₂O₃ thin films, Appl. Phys. Lett. **77**, 4166 (2000).

^[9] K. Sasaki, A. Kuramata, T. Masui, E. G. Víllora, K. Shimamura, and S. Yamakoshi, Device-quality β-Ga₂O₃ epitaxial films fabricated by ozone molecular beam epitaxy, Appl. Phys. Express 5, 035502 (2012).

^[10] A. J. Green, K. D. Chabak, E. R. Heller, R. C. Fitch, M. Baldini, A. Fiedler, K. Irmscher, G. Wagner, Z. Galazka, and S. E. Tetlak, 3.8-MV/cm breakdown strength of MOVPE-Grown Sn-doped β-Ga₂O₃ MOSFETs, IEEE Electron. Device Lett. 37, 902 (2016).

- [13] Q. D. Ho, T. Frauenheim, and P. Deák, Theoretical confirmation of the polaron model for the Mg acceptor in β -Ga₂O₃, J. Appl. Phys. **124**, 145702 (2018).
- [14] H. Peelaers, J. L. Lyons, J. B. Varley, and C. G. Van de Walle, Deep acceptors and their diffusion in Ga₂O₃, APL Mater. **7**, 022519 (2019).
- [15] K. H. L. Zhang, K. Xi, M. G. Blamire, and R. G. Egdell, *P*-type transparent conducting oxides, J. Phys.: Condens. Matter. 28, 383002 (2016).
- [16] H.-X. Deng, J.-W. Luo, and S.-H. Wei, Band structure engineering and defect control of oxides for energy applications, Chin. Phys. B 27, 117104 (2018).
- [17] G. Brunin, F. Ricci, V.-A. Ha, G.-M. Rignanese, and G. Hautier, Transparent conducting materials discovery using high-throughput computing, npj Comput. Mater. 5, 63 (2019).
- [18] H. Kawazoe, M. Yasukawa, H. Hyodo, M. Kurita, H. Yanagi, and H. Hosono, *P*-type electrical conduction in transparent thin films of CuAlO₂, Nature **389**, 939 (1997).
- [19] H. Hiramatsu, K. Ueda, H. Ohta, M. Hirano, M. Kikuchi, H. Yanagi, T. Kamiya, and H. Hosono, Heavy hole doping of epitaxial thin films of a wide gap *p*-type semiconductor, LaCuOSe, and analysis of the effective mass, Appl. Phys. Lett. 91, 012104 (2007).
- [20] W.-J. Yin, S.-H. Wei, M. M. Al-Jassim, J. Turner, and Y. Yan, Doping properties of monoclinic BiVO₄ studied by first-principles density-functional theory, Phys. Rev. B 83, 155102 (2011).
- [21] A. Bhatia, G. Hautier, T. Nilgianskul, A. Miglio, J. Sun, H. J. Kim, K. H. Kim, S. Chen, G.-M. Rignanese, X. Gonze, and J. Suntivich, High-mobility bismuth-based transparent *p*-type oxide from high-throughput material screening, Chem. Mater. 28, 30 (2015).
- [22] J. Heyd, G. E. Scuseria, and M. Ernzerhof, Hybrid functionals based on a screened Coulomb potential, J. Chem. Phys. 118, 8207 (2003).
- [23] G. Kresse and J. Furthmüller, Efficient iterative schemes for *ab initio* total-energy calculations using a plane-wave basis set, Phys. Rev. B **54**, 11169 (1996).
- [24] L. G. Sillén, On the crystal structure of monoclinic α -Bi₂O₃, Z. Kristallogr. **103**, 274 (1941).
- [25] K. R. Gbashi, A. A. Najim, M. A. H. Muhi, and A. T. Salih, Structural, morphological, and optical properties of nanocrystalline $(Bi_2O_3)_{1-x}$: $(TiO_2)_x$ thin films for transparent electronics, Plasmonics 14, 623 (2018).

- [26] T. Wang, W. Li, C. Ni, and A. Janotti, Band Gap and Band Offset of Ga_2O_3 and $(Al_xGa_{1-x})_2O_3$ Alloys, Phys. Rev. Appl. **10**, 011003(R) (2018).
- [27] S.-H. Wei, L. G. Ferreira, J. E. Bernard, and A. Zunger, Electronic properties of random alloys: Special quasirandom structures, Phys. Rev. B **42**, 9622 (1990).
- [28] S.-H. Wei and S. B. Zhang, Chemical trends of defect formation and doping limit in II-VI semiconductors: The case of CdTe, Phys. Rev. B **66**, 155211 (2002).
- [29] C. Freysoldt, B. Grabowski, T. Hickel, J. Neugebauer, G. Kresse, A. Janotti, and C. G. Van de Walle, First-principles calculations for point defects in solids, Rev. Mod. Phys. 86, 253 (2014).
- [30] C. Freysoldt, J. Neugebauer, and C. G. Van de Walle, Fully *Ab Initio* Finite-Size Corrections for Charged-Defect Supercell Calculations, Phys. Rev. Lett. **102**, 016402 (2009).
- [31] P. Deák, Q. D. Ho, F. Seemann, B. Aradi, M. Lorke, and T. Frauenheim, Choosing the correct hybrid for defect calculations: A case study on intrinsic carrier trapping in β -Ga₂O₃, Phys. Rev. B **95**, 075208 (2017).
- [32] See Supplemental Material at http://link.aps.org/supplemental/ 10.1103/PhysRevB.103.115205 for the results of further accuracy and convergence studies, and for the test results for position of the dopant in the alloy.
- [33] H. Peelaers and C. G. Van de Walle, Brillouin zone and band structure of β-Ga₂O₃, Phys. Status Solidi B **252**, 828 (2015).
- [34] K. Yamaguchi, First principles study on electronic structure of β-Ga₂O₃, Solid State Commun. **131**, 739 (2004).
- [35] A. Mock, R. Korlacki, C. Briley, V. Darakchieva, B. Monemar, Y. Kumagai, K. Goto, M. Higashiwaki, and M. Schubert, Band-to-band transitions, selection rules, effective mass, and excitonic contributions in monoclinic β -Ga₂O₃, Phys. Rev. B **96**, 245205 (2017).
- [36] R. D. Shannon, Revised effective ionic radii and systematic studies of interatomic distances in halides and chalcogenides, Acta Crystallogr. **32**, 751 (1976).
- [37] B. E. Kananen, N. C. Giles, L. E. Halliburton, G. K. Foundos, K. B. Chang, and K. T. Stevens, Self-trapped holes in β -Ga₂O₃ crystals, J. Appl. Phys. **122**, 215703 (2017).
- [38] Y. Zhang, J. Yan, Q. Li, C. Qu, L. Zhang, and W. Xie, Optical and structural properties of Cu-doped β -Ga₂O₃ films, Mater. Sci. Eng. B **176**, 846 (2011).
- [39] H. Yan, Y. Guo, Q. Song, and Y. Chen, First-principles study on electronic structure and optical properties of Cu-doped β -Ga₂O₃, Phys. B (Amsterdam, Neth.) **434**, 181 (2014).